High Resolution, Fluorescence Deconvolution Microscopy and Tagging With the Autofluorescent Tracers CFP, GFP, and YFP to Study the Structural Composition of Gap Junctions in Living Cells

MATTHIAS M. FALK* AND UNDINE LAUF
Department of Cell Biology, The Scripps Research Institute, La Jolla, California 92037

KEY WORDS connexins; fluorescent proteins; membrane proteins; oligomers; reporter technology

ABSTRACT High-resolution, fluorescence deconvolution (DV) microscopy was implemented to obtain a detailed view of the organization and structural composition of gap junctions assembled from one or two different connexin isotypes in live and fixed cells. To visualize gap junctions, the structural protein components of gap junction channels, the connexin polypeptides α_1(Cx43), β_1(Cx32), and β_2(Cx26), were tagged on their C-termini with the autofluorescent tracers green fluorescent protein (GFP), and its cyan (CFP), and yellow (YFP) color variants. Tagged connexins were expressed in transiently transfected HeLa cells. Comprehensive analysis including dye-transfer analysis demonstrated that the tagged connexins trafficked, assembled, and packed normally into functional gap junction channel plaques. Such gap junction plaques were examined by single, dual, and triple-color DV microscopy. High-resolution images and three-dimensional volume reconstructions of gap junction plaques were obtained by this technique, which revealed several new aspects of gap junction structure. Specifically, the studies demonstrated that the mode of channel distribution strictly depends on the connexin isotypes. Here we present such images, and volume reconstructions in context with images obtained by other light, and electron microscopic techniques, such as laser scanning confocal, conventional wide-field fluorescence, thin section, and freeze-fracture electron microscopy. In addition, we give a simple description of the principal mechanisms of DV microscopy, name advantages and disadvantages, and discuss issues such as dual-color imaging using CFP and YFP, spatial resolution, colocalization, and avoiding imaging artifacts. *Microsc. Res. Tech. 52:251–262, 2001.*

INTRODUCTION

The past few years have seen a revival of fluorescence microscopy, in particular due to the recent availability of autofluorescent tracer proteins, such as green fluorescent protein (GFP), isolated and cloned from the northwest Pacific cold-water jellyfish *Aquorea victorea* (Inouye and Tsuji, 1994; Prasher et al., 1992). The many potential uses of GFP, including the possibility to observe the behavior of proteins in live cells, was quickly recognized, and triggered the development of novel GFP variants, with specific characteristics, such as improved fluorescence brightness (Heim and Tsien, 1996), shifted excitation and emission spectra (Heim et al., 1995; Yang et al., 1998), organelle specific targeting (Rizzuto et al., 1996), reduced half-live (Anderson et al., 1998; Li et al., 1998) or intrinsic properties that sense environmental changes (Miyawaki et al., 1997; Miesenböck et al., 1998), as well as a frantic search for other autofluorescent proteins with different properties to GFP (Matz et al., 1999; Heikal et al., 2000; Baird et al., 2000; Terskikh et al. 2000; Wall et al., 2000; Gross et al., 2000; reviewed in Tsien, 1999; Chicurel, 2000). This process went hand in hand with the development of more light-sensitive devices, such as cooled charge-coupled device (CCD) cameras, faster processing hardware and software that could handle large image-files, and the development, improvement, and commercialization of novel imaging systems.

We have used a fluorescence-enhanced GFP variant (EGFP), and its cyan (ECFP) and yellow (EYFP) color variants as autofluorescent reporters, and combined this approach with single, double, and triple-color fluorescence, high resolution, deconvolution (DV) microscopy, to study the structure and function of gap junctions.

Gap junctions represent more or less tightly packed two-dimensional aggregates of individual channels that cluster together to create characteristic gap junction plaques, structurally distinguishable from other clustered arrangements of particles also present in the plasma membrane (Friend and Gilula, 1972; McNutt and Weinstein, 1970; Rash et al., 1974). Typically, less than a hundred to many thousand individual channels

Contract grant sponsor: National Institute of Health; Contract grant number: RO1 GM55725.

*Correspondence to: Matthias M. Falk, Ph.D., Department of Cell Biology, MB21, The Scripps Research Institute, 10550 North Torrey Pines Road, La Jolla, CA 92037. E-mail: mfalk@scripps.edu

Received 15 March 2000; accepted in revised form 12 June 2000

are combined in a single plaque that can extend from less than a hundred nanometers to several micrometers in diameter (McNutt and Weinstein, 1970).

Gap junction channels represent double-membrane protein-structures that create hydrophilic pores across the membranes (Makowski et al., 1977). The channels mediate direct cell-to-cell communication by allowing the passage of small biological molecules (up to approximately 1 kDa in size) from one cell to the other (Gilula et al., 1972). In mammals, gap junction channels have been characterized to be composed of two hemi-channels, termed connexons, each provided by one of the two neighboring cells. Two connexons "pair" in the adjoining plasma membranes to form the complete, double-membrane intercellular junction. Each connexon is composed of 6 polytopic transmembrane protein subunits, termed connexins. At least 14 different connexin isotypes have now been cloned and sequenced from mice. All represent structurally conserved nonglycosylated members of a multigene family that mainly differ in the length of their C-terminal domain. Although the different connexin isotypes exhibit a distinct tissue distribution, many cell types express more than one connexin isotype. This may allow the assembly of hetero-oligomeric connexons constructed from different connexin isotypes, in addition to the assembly of homo-oligomeric connexons constructed from a single connexin isotype (for a structural review, see Kumar and Gilula, 1996). It appears obvious that connexin protein synthesis and assembly, intracellular trafficking, and channel formation are important steps in the maturation process of gap junctions that have to be coordinated and regulated precisely to enable proper channel function.

Previously, we have studied the synthesis and assembly of connexins into connexons. The studies have shown that the connexin subunits are cotranslationally integrated into the endoplasmic reticulum (ER) membrane in a process that is similar to the process described for other transmembrane proteins (Falk et al., 1994). There, they adapt their native transmembrane configuration traversing the membrane bilayer four times with N- and C-termini located in the cytoplasm (Falk and Gilula, 1998). The studies further demonstrated that connexins can assemble into functional hexameric connexons in the ER membrane (Falk et al., 1997). Sub-cellular fractionation studies (Falk et al., 1994; Musil and Goodenough, 1991) and immuno-colocalization analyses (Laird et al., 1995; Musil and Goodenough, 1991; Falk, 2000c) indicated that connexins traffic through the Golgi apparatus to reach the plasma membrane. There, the connexons pair into the complete double-membrane channel structures, and channels cluster together into gap junction plaques (reviewed in Falk, 2000a,b; Yeager et al., 1998).

For the present study, three different connexin isotypes were tagged on their C-terminal ends with CFP, GFP, or YFP. The reporters were fused to the C-terminus of connexins, since earlier studies have shown that their C-terminal domain tolerates some flexibility. Deletions (Unger et al., 1999), as well as additions (Sullivan and Lo, 1995) to the C-terminus of connexin subunits were possible without interfering with the intracellular transport, or disrupting assembly of the mutated subunits into gap junction channels and gap junction plaques.

In general, GFP was found not to interfere with the normal behavior of tagged proteins. This inert behavior of the GFP tag was attributed to its unique tightly packed can-shape structure (Misteli and Spector, 1997). Comprehensive analysis (reported in Falk, 2000c) demonstrated that all three tagged connexin isotypes trafficked and assembled normally into functional gap junction channels and gap junction plaques. Our results are supported by the findings of Jordan et al. (1999) and Holm et al. (1999) who also observed that a fusion protein consisting of GFP fused to the C-terminus of α_1(Cx43) assembled into functional gap junction channels.

Here we report novel results on the structural organization and composition of gap junctions that were obtained by implementing high-resolution DV microscopy in combination with a tagging approach that used the autofluorescent reporters CFP, GFP, and YFP. The results are presented in context with results obtained by other light and electron microscopic techniques. In addition, we give a simple description of the principal mechanisms of DV microscopy, name advantages and disadvantages, and briefly discuss issues such as dual-color imaging using CFP and YFP, spatial resolution, and avoiding severe imaging artifacts. The goal of this article is to provide some educational information to potential microscopy users to help in choosing the technique that best accomplishes their needs.

MATERIALS AND METHODS

Connexin-CFP, GFP, and YFP cDNA Constructs

Connexin cDNAs, lacking their STOP-codon, were digested with *Eco*RI and *Bam*HI, and cloned into the *Eco*RI and *Bam*HI restricted vectors pEGFPN1, pECFPN1, and pEYFPN1 (Clontech, Palo Alto, CA) as described in Falk, (2000c). The resulting connexin constructs contained the complete connexin specific coding sequence, a seven amino acid linker (Ala-Asp-Pro-Pro-Val-Ala-Thr), and the GFP, CFP, or YFP coding sequences, respectively.

Cell Line, Cell Culture, and Transfection Conditions

Human epitheloid cervix carcinoma cells (HeLa, ATCC CCL 2; American Type Culture Collection, Rockville, MD) transiently transfected with the tagged connexin constructs were used throughout this study. They have been shown to efficiently assemble functional gap junctions when transfected with connexin specific cDNAs (Elfgang et al., 1996); they do not express endogenous α_1(Cx43), β_1(Cx32), or β_2(Cx26) (Eckert et al., 1993; Elfgang et al., 1996; Hülser et al., 1997), and their growth is not inhibited upon contact. This results in the formation of gap junction plaques that can be viewed on their surface, besides the more common view on the edge of the plaques. Cells were maintained in high glucose Dulbecco Minimum Essential Medium (DMEM), supplemented with 10% fetal calf serum and 100 U of penicillin and streptomycin per ml. For transient transfection, cells were split and seeded the day prior to transfection to reach 60–70% confluency. Cells were transfected with Superfect Transfection Reagent (Qiagen, Valencia, CA) following

the manufacturer's instructions. Transfection efficiencies of 10–30% were regularly obtained.

Immunofluorescence Staining

For indirect immunofluorescence microscopy of gap junctions, or the Golgi complex, Hela cells were seeded on number 1 glass coverslips treated overnight with a 0.01% poly-L-lysine solution diluted with water from a 0.1% stock solution (Sigma Diagnostics Inc. St. Louis, MO). Transfected cells were grown overnight, fixed for 10 min at RT in 2% formaldehyde (Polysciences Inc. Warrington, PA), permeabilized in ice cold acetone (5 min at −20°C), blocked (30 min at RT in PBS containing 1% bovine serum albumine), washed 3 times in PBS, and incubated with primary antibodies diluted in PBS containing 0.5% BSA (1 hour at RT). Purified α_1(Cx43) specific polyclonal antipeptide antibodies (α_1S) (Milks et al., 1988) (kindly provided by N.B. Gilula, The Scripps Research Institute, La Jolla, CA), monoclonal anti p58K protein antibodies (Sigma), and polyclonal anti-Mannosidase II antibodies (kindly provided by K. Moremen, University of Georgia, Athens, GA) were used in 1:100 dilution. Texas Red coupled goat anti rabbit, and FITC coupled goat anti mouse (Jackson Laboratories, West Grove, PA), respectively, were used as secondary antibodies at 1:200 dilution. Nuclei were stained with DAPI prior to mounting in Fluoromount-G (Southern Biotechnology Associates Inc., Bermingham, AL).

Microscopy Techniques

Conventional Wide-Field Fluorescence Microscopy. Fixed cells were examined with an upright Zeiss Axiophot wide-field fluorescence microscope equipped with a 100× (Plan-Neofluar, NA 1.30 oil immersion) objective lens and standard filter sets. Single, double, and triple exposures were imaged on Kodak 1600 ASA slide film.

Laser Scanning Confocal Microscopy. Fixed and live cells were imaged with a Bio-Rad MRC1024 confocal microscope system attached to an inverted Zeiss Axiovert S100TV wide-field fluorescence microscope. Optical sections of gap junction plaques assembled from GFP tagged connexins were collected in 0.2-μm steps covering the entire z-axis field of 4–10 μm, using a 100× (Plan-Neofluar, NA 1.30 oil immersion) objective lens. (Specific settings were Box-size 515×512, zoom 3, iris 3, gain 1500, Black level 0, laser power 1%.) Images were captured with the attached photomultiplier tubes (PMTs). Images were displayed, and volume reconstructions were rendered using the Bio-Rad Lasersharp software package (Version 3.2). Images were stored on CD-ROM.

Deconvolution Microscopy and Image Processing. A DeltaVision Model 283 (Applied Precision Inc., Issaquah, WA) was used to obtain high-resolution images and three-dimensional volume reconstructions of gap junctions, and Golgi membranes. This system uses a wide-field optical sectioning microscope for image acquisition and subsequent computational image processing to increase resolution. Fixed cells were imaged on standard microscope slides embedded as described above. For live cell imaging HeLa cells were seeded on round, 40-mm diameter glass coverslips (Bioptechs Inc. Butler, PA) coated overnight with poly-L-lysine (Sigma), and were transfected with tagged connexins. Next day, coverslips were mounted in a closed live cell chamber (Focht Live-Cell Chamber System FCS2, Bioptechs Inc.) using phenolred-free DMEM (Gibco BRL, Grand Island, NY). Temperature was kept constant at 37°C using the attached automatic FCS2 temperature controller. A Kodak Photometrics, CH350L liquid cooled charged coupled device (CCD) camera (500 KHz, 12 bit, 2MP, KAF1400GI, 1,317 × 1,035 pixels) was used for imaging, attached to an inverted Olympus IX-70 wide-field fluorescence microscope. The autofluorescent proteins CFP, GFP, and YFP were excited with a standard mercury arc lamp attached to a fiber optic illumination scrambler providing even illumination. GFP and FITC fluorescence were detected using a standard FITC filter set, Texas Red fluorescence was detected using a standard rhodamine/Texas Red filter set. CFP and YFP fluorescence was imaged alternating by exchanging filters mounted in a filter wheel. An 86002-filter set (CFPex 436/10, CFPem 470/30, YFPex 500/20, YFPem 535/30, Chroma Technology Corp., Brattleboro, VT) was used. Optical sections of gap junction plaques assembled from CFP, GFP, and YFP tagged connexins were generally acquired at maximum magnification (Plan-Apochromat 100×, NA 1.35 oil immersion lens, plus 1.5× auxiliary magnification). Section planes were collected in 0.1–0.2-μm steps covering the entire z-axis field of 5–10 μm using the Applied Precision Inc. motorized stage. Images were acquired setting binning, and gain of the CCD camera to 1, resulting in a minimum pixel size that corresponds to 44.8 × 44.8 nm of the specimen. In some experiments, the relatively low signal and bleaching of CFP required to set the gain to 4 to obtain decent exposure times. In general, 0.2–0.5-second exposure times were required to obtain sufficiently saturated images suitable for deconvolution (≥ 1,100 gray levels, dynamic range of the cooled CCD camera was 0–4095) with GFP, FITC, and Texas Red. Exposure times were between 0.2–1 second for YFP, and 2–5 second for CFP. Images were saved and processed on attached Silicon Graphics workstations (O2, Octane) using the DeltaVision software package *softWoRx* (Version 2.5), stored on CD-ROM, and finalized with Photoshop (version 5.02, Adobe Systems Incorporated, San Jose, CA) on a MacIntosh G3 (Apple Computer Inc., Cupertino, CA).

RESULTS

Structural Organization of Gap Junctions Revealed by High-Resolution Fluorescence DV Microscopy

HeLa cells were transiently transfected with GFP tagged α_1 (Cx43). Cell-pairs with gap junction plaques assembled in their adjoining membranes were imaged using either a DV microscope, a laser scanning confocal microscope, or a conventional wide-field fluorescence microscope. To obtain images of complete gap junction plaques, a set of z-sections spaced 0.2 μm apart was acquired with the DV microscope, and with the confocal microscope, respectively, that covered the entire depth of a plaque. Images acquired with the DV microscope were deconvolved. Volume reconstructions of the gap junction plaques were rendered from the z-section stacks acquired with the DV, and the confocal microscope, respectively. Conventional fluorescence wide-

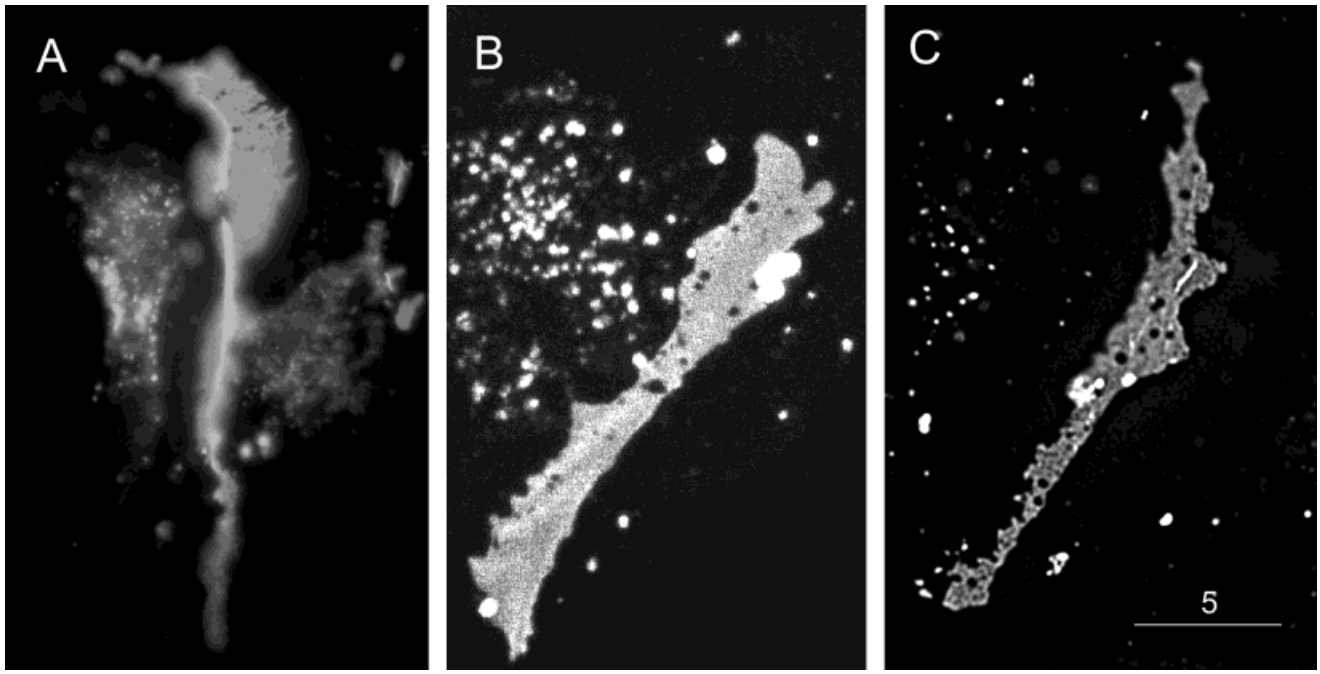

Fig. 1. Structural organization of gap junctions. Large gap junctions, as, for example, present in otocyst sensory epithelium, undifferentiated epidermis, and inner ear, were imaged at high primary magnification (100× lens) by conventional wide-field fluorescence microscopy (**A**), laser scanning confocal microscopy (**B**), and using a wide-field deconvolution microscope system (**C**), after expressing GFP-tagged α, (Cx43) in transfected HeLa cells. Structural details of the gap junctions (see text) are visible in all three images. Structural details of the gap junction plaques were resolved best in the deconvolved image. The conventional fluorescence image shows some blur due to out-of-focus fluorescence, and the confocal image is relatively low in contrast and therefore appears somewhat "grainy." Bars = 5 μm.

field microscopes collect the entire thickness of the sample in one image. Large gap junction plaques, such as present in chicken otocyst sensory epithelium (Ginzberg and Gilula, 1979), embryonic epidermis (Risek et al., 1994), and between cells of the inner ear (Andrew Forge, University College London, personal communication), predominantly visible onto their plane, were imaged with a conventional wide-field fluorescence microscope (Fig. 1A), imaged with a laser scanning confocal microscope (Fig. 1B), and imaged with a DV microscope system (Fig. 1C). With all three techniques, gap junction plaques were clearly detected in the adjoining plasma membranes of neighboring cells. Structural details (described below) of the plaques can bee seen with all three systems when plaques were imaged at a high primary magnification. The plaques imaged with the conventional wide-field fluorescence microscope showed some background blur predominantly due to out-of-focus fluorescence (Fig. 1A), whereas the image obtained by confocal microscopy appeared "grainy" (see below) (Fig. 1B). In this comparison, the image obtained with the DV microscope showed the highest resolution (for technical description of the systems see Discussion) (Fig. 1C). Note that the shape of the plaques is quite irregular. The edges of the plaques appear wavy and jagged. Sometimes, long extending protrusions (compare Fig. 2B) or deep invaginations devoid of gap junction channels (compare Fig. 1A) can be seen on their edges. Fluorescent vesicles were found in close proximity to the plaques and further away in the cytoplasms of the cells that may represent transport vesicles, and/or partial plaque degradation products. Finally, circular, and sometimes irregularly shaped areas (approximately 0.1– 1 μm in diameter), not containing gap junction channels, were detected in all three images within the plaques (Fig. 1A–C). They were resolved best in the deconvolved images. The characteristics described above were also seen in smaller (≤ 2 μm diameter) gap junction plaques, in gap junction plaques that were assembled in stable transfected cell lines, as well as in plaques assembled from untagged and endogenously expressed connexins (compare Figs. 4A, and 6). All images presented in this comparison were acquired with 100× lenses. One should mention here that the different microscope types, objective lenses, and recording systems used in this comparison may influence the quality of the images, and therefore, should be similar for a truly realistic comparison. Furthermore, completely optimized adjustments of the individual microscope systems may have resulted in images with an even higher quality.

Three-Dimensional Volume Rendering of Gap Junction Plaques

Computational image processing using advanced computer software was used to render three-dimensional volume reconstructions of gap junction plaques captured with the DV-microscope system. For that purpose, z-sections were acquired from gap junction plaques covering the entire depth of the plaques with

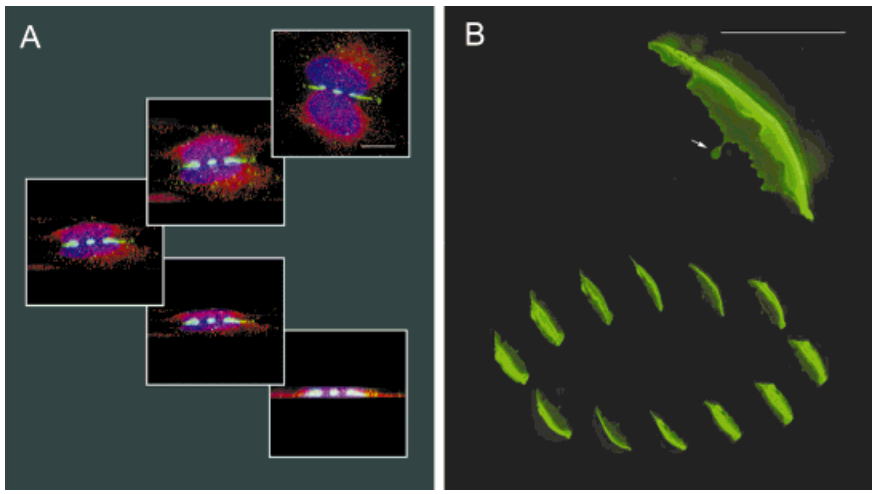

Fig. 2. Volume rendering of gap junction plaques. Three-dimensional views of gap junction plaques assembled from α_1(Cx43) in fixed cells (**A**) and in live cells (**B**) were rendered by sampling a stack of images spaced 0.2 μm apart covering the entire depth of the plaques. Images were deconvolved, volume views were reconstructed from the image stacks using *softWoRx* computer software, and rotated 180° (A), or 360° (B) around their longitudinal axis. Representative tilt projections are shown. Such volume reconstructions provide a true, three-dimensional impression of entire gap junction plaques as they appear in the adjoining membranes between cells. Note the small area of the gap junction plaque (marked with an arrow in B) that is only connected with the large plaque by a thin bridge that is only a few channels wide. Nuclei are stained blue, endoplasmic reticulum is stained red, and gap junctions assembled from GFP tagged α_1(Cx43) are green. Note that gap junction plaques in the 90° tilted image (A) appear yellow and white, due to the overlay of green and red, or red, green, and blue, respectively. Bars = 10 μm.

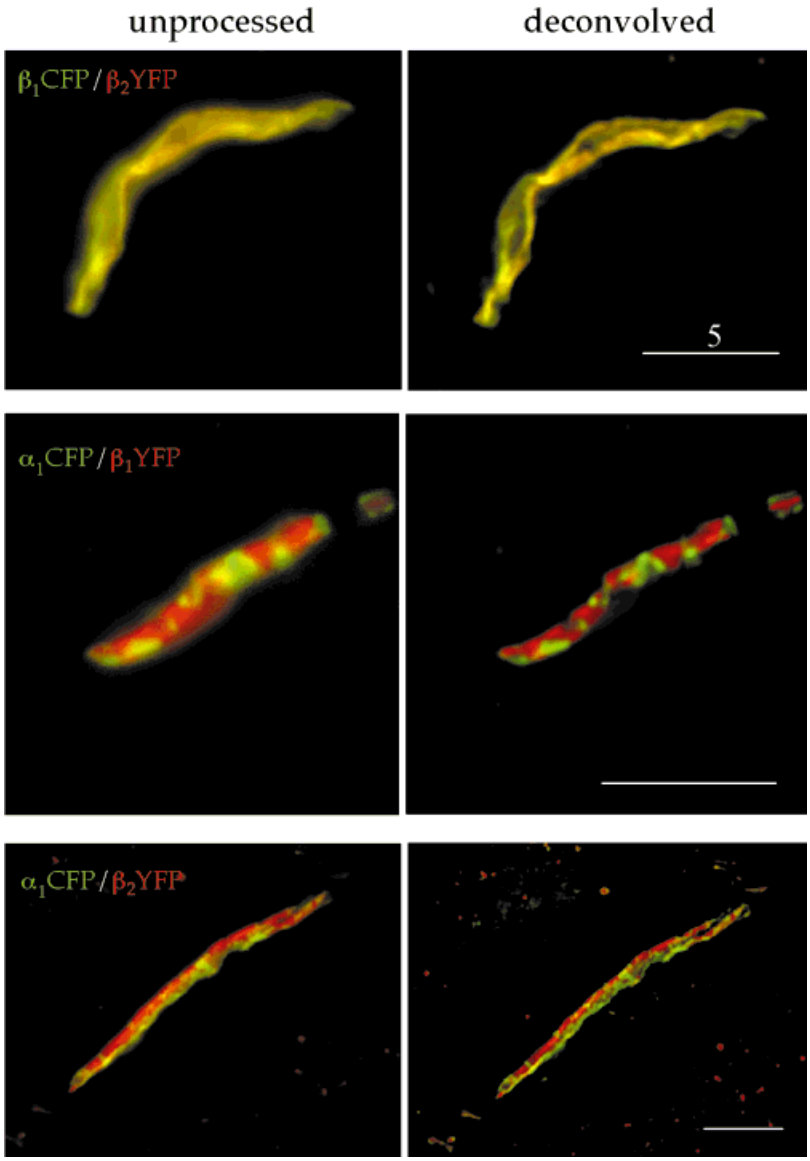

Fig. 3. Structural composition of gap junctions in live cells assembled from two different connexin isotypes. Connexin isotypes α_1(Cx43), β_1(Cx32), and β_2(Cx26) were tagged with the autofluorescent reporter proteins CFP and YFP, respectively. HeLa cells were cotransfected in all possible double-combinations, and assembled plaques were imaged together at high primary magnification. In the images, CFP emission was pseudocolored green, and YFP emission was pseudocolored red. Representative images are shown unprocessed (**left**) and after deconvolution (**right**). Connexin isotypes sharing the same characteristics (β_1[Cx32] plus β_2[Cx26]) assembled into hetero-oligomeric channels composed of both connexin isotypes, or into mixed homo-oligomeric channels (red and green, appearing homogenously yellow), while connexin isotypes with different characteristics (α_1[Cx43] plus β_1[Cx32], and α_1[Cx43] plus β_2[Cx26]) assembled into well-separated domains (red or green). Note how the deconvolution process increases image resolution. Bars = 5 μm.

an image spacing of 0.2 μm. All frames of the image-stacks were deconvolved, three-dimensional volume reconstructions generated from the z-section stacks using *softWoRx* computer software, which then were rotated around their longitudinal axis (Fig. 2A and B). Such volume reconstructions provide a realistic, three-dimensional impression of entire gap junction plaques as they appear in the adjoining plasma membranes between living cells. Structural details described above were also visible in the volume reconstructions. That gap junction plaques appearing as one-dimensional puncta and lines in an edge-on view indeed represent two-dimensional sheets that extend throughout the plain of the membranes can be demonstrated by this technique as well.

Dual-Color, Live-Cell DV Microscopy of Gap Junction Plaques

To obtain detailed information on the structural composition of gap junction plaques assembled from two different connexin isotypes, α_1(Cx43), β_1(Cx32), and β_2(Cx26) were tagged with the GFP color variants ECFP and EYFP, respectively, and were imaged together in cotransfected live HeLa cells. CFP tagged connexins were pseudocolored green, and YFP tagged connexins were pseudocolored red. Unprocessed and deconvolved images of representative plaques are shown in Figure 3. When CFP-tagged β_1(Cx32) was cotransfected with YFP tagged β_2(Cx26), the two proteins were distributed homogenously throughout the plaque resulting in yellow colored plaques (Fig. 3, top). When tagged α_1(Cx43), and β_1(Cx32), or α_1(Cx43) and β_2(Cx26) were coexpressed, still both proteins trafficked to the same gap junction plaques, but assembled into well separated domains (green, or red) consisting of either connexin isotype (Fig. 3, middle and bottom). Identical results were obtained when tags were exchanged (not shown). These results suggest that coexpressed connexins sharing yet unknown characteristics may assemble into hetero-oligomeric, and probably hetero-typic channels, while coexpressed connexins with different characteristics only oligomerize into homo-oligomeric and homo-typic channels, and only assemble into well-separated domains. This hypothesis is consistent with results published previously by us, and others, investigating the homo- and hetero-oligomeric composition of connexons, and complete gap junction channels by biochemical, immunological, and electrophysiological approaches (Brink et al., 1997; Falk et al., 1997; He et al., 1999; Jiang and Goodenough, 1996; Stauffer, 1995).

In general, more or less extensive yellow areas were present in our unprocessed images of the plaques assembled from α and β subclass connexins that would suggest a homogenous mixing of the two connexin, or channel types in these areas of the plaques (Fig. 3, unprocessed images, middle and bottom). However, these yellow areas disappeared, or were reduced to narrow borders located only between green and red domains after the images were deconvolved (Fig. 3, deconvolved images, middle and bottom). The enhancement of the image resolution by the deconvolution process (see below) indicates that domains consisting of mixed channel populations do not exist in these α/β plaques, and the appearance of yellow is an imaging artifact, generated by the limited spatial resolution of light microscopic techniques. An efficient and complete separation into either hetero- or homo-oligomeric gap junction channel types appears convincing if a specific signal, responsible for connexin subunit recognition and assembly, is located in the connexin polypeptides. In previous studies, we have found such signals that are required for assembly and selectivity of different connexin isotypes (Falk et al., 1997; 1998; reviewed in Falk, 2000a,b; Yeager et al., 1998).

DISCUSSION

Previously, fluorescently labeled gap junctions, in general, were imaged at relatively low magnification. At low magnification, gap junction plaques appear as somewhat blurry lines and puncta between cells (compare Fig. 2A) and no structural details are resolved. For the current study, we have imaged gap junctions at a higher primary magnification in the absence of fixatives in living cells (Figs. 1, 2B, 3, 4A) and compared the results with images obtained from fixed cells (Figs. 2A, 4A; see also Fig. 6). In addition, the acquired images were deconvolved to even better resolve the structural and organisatorial features of gap junction plaques.

Dual-Color Live Cell Microscopy Using CFP and YFP

To obtain more detailed information on the structural composition of gap junction plaques assembled from two different connexin isotypes, α_1(Cx43), β_1(Cx32), and β_2(Cx26) were tagged with the GFP color variants ECFP and EYFP, respectively, and were imaged together in cotransfected live HeLa cells. The excitation and emission spectra of ECFP (ex. max. = 433 nm; em. max. = 475 nm) and EYFP (ex. max. = 513 nm; em. max. = 527 nm) lie far enough apart from each other so that newly developed specific filter sets now sufficiently allow to separately excite and record the emitted light. However, because of the overlapping emission spectra of CFP and YFP, results obtained should be accompanied by relevant controls. For example, CFP emission bleeding into the YFP channel may occur and should be checked for. The reduced brightness and relatively fast bleaching nature of the CFP variant can pose further problems when larger numbers of exposures will be acquired. Excitation and emission spectra of EGFP (ex. max. = 488 nm, em. max. = 509 nm) lie in between the spectra of CFP and YFP, and make this variant not suitable for dual imaging with either CFP or YFP. Another color variant of GFP, blue fluorescent protein (BFP) is commercially available (Clonetech; Quantum Biotechnologies Inc.), which has excitation and emission spectra further shifted to blue light (ex. max. = 380 nm; em. max. = 440 nm) that allows double imaging with GFP. However, its very rapid bleaching does not allow multiple exposures and, therefore, it is not very useful for DV and confocal microscopy, and volume rendering, or time lapse imaging (M. Falk, unpublished results). The availability of novel autofluorescent proteins, such as the now commercially available DsRed (Clontech) isolated from the IndoPacific sea anemone relative *Discosoma spec.* (Matz et al., 1999), may in future prove useful for gap junction research and the above-mentioned techniques.

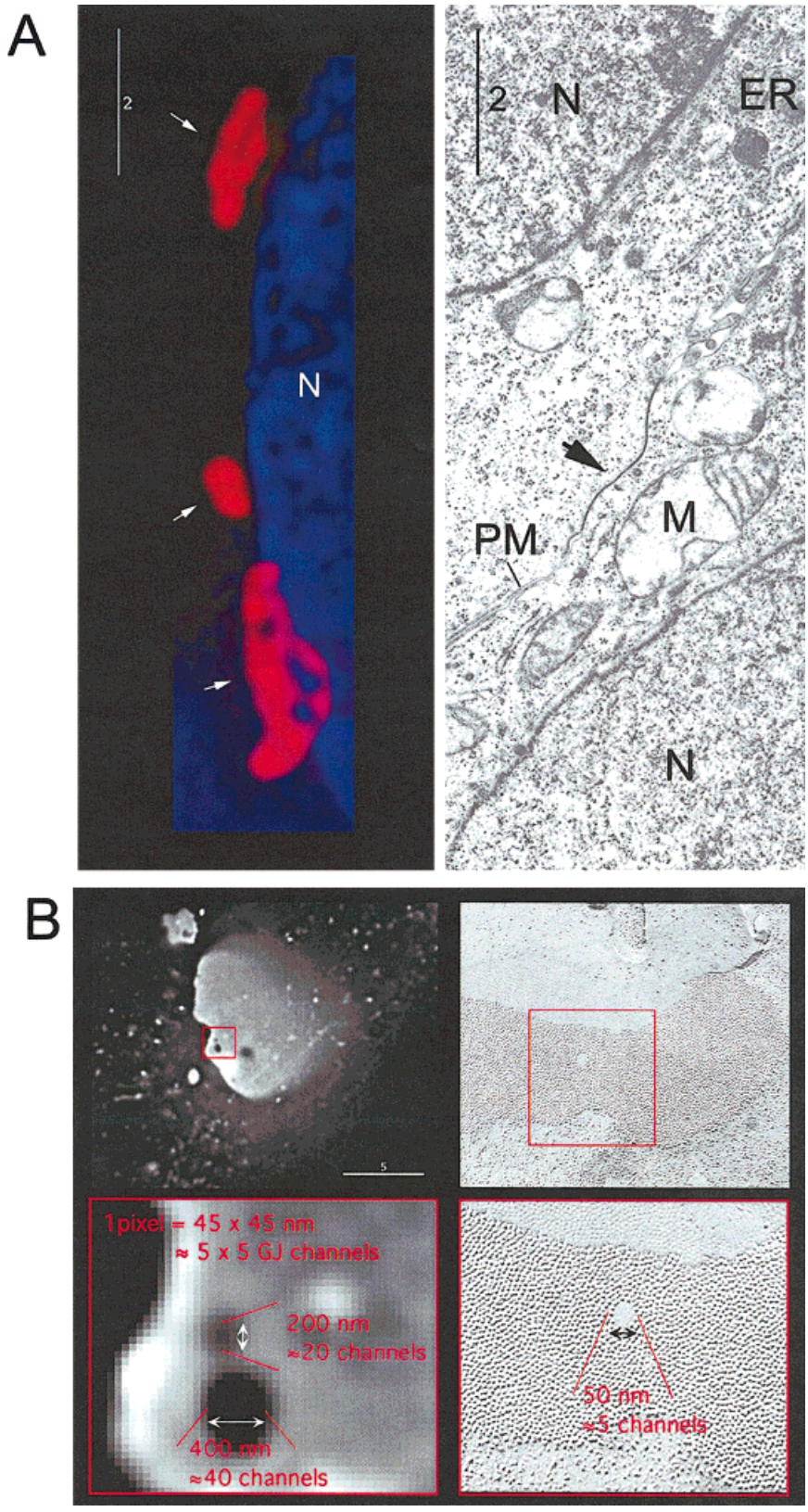

Fig. 4. Spatial resolution of gap junctions achieved with deconvolution microscopy. To demonstrate the maximal spatial resolution that we achieved with the deconvolution (DV) microscope system implemented in this study, gap junction plaques (marked with arrows) are shown in comparison to gap junction plaques that were imaged with an electron microscope. **A:** On the left, gap junctions endogenous to glial cells were stained with an α_1(Cx43) specific antibody in combination with a Texas Red coupled secondary antibody (red) and imaged at maximal primary magnification (100× lens, plus 1.5× auxiliary magnification). Nuclei were stained with DAPI (blue). On the right, thin-sectioned cells imaged with an electron microscope (EM) are shown at the same final magnification (space bars in both images represent 2 μm). The gap junction plaque in the EM image corresponds in size to the large gap junction at the bottom of the DV image. The smaller gap junction plaques correspond in size to mitochondria (M). Structural features, including nonjunctional membranes, were resolved. Note that the gap junctions imaged with the DV microscope are seen in a planar view, whereas the plaque imaged with the EM is seen on edge. ER, endoplasmic reticulum; N, nuclei; PM, plasma membrane. **B:** On the left two gap junction plaques are shown assembled from GFP-tagged α_1(Cx43) in transfected HeLa cells. Nonjunctional membranes present within the plaques appear as dark holes in the labeled planar views of the plaques. Plaques were imaged at maximal magnification (100× lens, 1.5× auxiliary magnification). The boxed area is shown below at higher secondary magnification. Pixels corresponding to individual light sensitive areas of the CCD camera photochip are clearly visible. At this maximal magnification, each pixel corresponds to a specimen area of 44.8 × 44.8 nm, or approximately 5 × 5 gap junction channels. The two nonjunctional membranes, localized approximately two pixels (~ 100 nm) apart, were clearly separated. On the right, an image of a gap junction freeze-fracture replica is shown in comparison at approximately 4 times higher final magnification. Note the central nonjunctional membrane that measures approximately 5 × 5 channels or 50 × 50 nm in diameter. Bars are in μm. [Color figure can be viewed in the online issue, which is available at www.interscience.wiley.com.]

Observation of proteins in live cells requires that the proteins be labeled with fluorescent probes. Such probes can, for example, be delivered to the cells via microinjection or by uptake. The cDNAs of autofluorescent reporter polypeptides, such as CFP, GFP, and YFP can be fused to the cDNAs encoding the proteins of interest and can be expressed simultaneously with them. Such autofluorescent protein probes have the advantage that they are highly specific and do not require cofactors to become fluorescent. Their use, however, requires that the DNA sequence encoding the target protein has been cloned. Although autofluorescent proteins can be useful in fixed cells as well, they are not required. A large group of fluorescent tracer molecules coupled to secondary antibodies are commercially available that emit fluorescence at different wavelengths covering the entire spectrum of visible light. Fluorescein (FITC) and Texas Red are the most popular stains. They are simpler to use for dual-color labeling experiments then CFP and YFP, since their excitation and emission spectra are located further apart, and they can be imaged with standard filter sets found in most fluorescence microscopes. Their use, however, requires that specific antibodies directed against the target protein are available. The effort, money, and time to produce a specific antiserum may be better invested than simply tagging the target protein with GFP. Although, in most cases completely inert, the GFP tag is quite large (24×42Å in diameter; Ormö et al., 1996) and may interfere with the normal behavior of the target protein as for example reported in Doyle and Botstein (1996), Dabiri et al. (1997), and Ayoob et al. (2000). A thorough comparative analysis of the fusion protein with the wild type, as was done for the current analysis (see Falk, 2000c), should always be performed to ensure the relevance of the obtained results.

Principles of DV Microscopy

Convolution is a mathematical term used to describe the process of mixing one function into another. Reversing this process (= de-convolution) separates the two functions and clarifies them. Deconvolution applied to fluorescence microscopy, is the process of relocating fluorescent blur to its source to enhance image resolution. In principal, every optical image, including images obtained by a confocal microscope, can be deconvolved, if sufficient information of the specimen and the optical system is available. The deconvolution microscope system implemented in this study uses a wide-field microscope for image acquisition as used in conventional wide-field fluorescence microscopy, to collect *all* of the fluorescent light that is emitted from a fluorophor. This is of great advantage if faint or rapidly bleaching labels will be imaged. This, however, causes fluorophores located above or below the optical plane of the objective lens to be excited and imaged as well, and thus generate blur by out-of-focus fluorescence. This can be seen, e.g., in the image of the gap junction plaque acquired by conventional wide-field fluorescence microscopy shown in Figure 1A. A second major factor-causing blur is related to the point spread function (PSF) of the objective lens used to image the object. The PSF describes the imaging characteristics of an objective lens. No optical lens system, regardless of its quality, can produce a perfect image of an object, since light will be scattered when passing through the optical system. This causes a light-point to be spread into a somewhat larger "light-ball." The goal of the deconvolution process is to improve image resolution by computationally shrinking the image of the light point to its original size, and to relocate the out-of-focus fluorescence to its source. Once the size of the image matches the size of the object, a satisfactory solution has been achieved (for reviews see Murray, 1998; Shaw, 1998). Small fluorescent beads of known size, computational estimates, and specific mathematical algorithms are used in this process. Although mathematical deconvolution algorithms were available for several years, the computationally intensive programs proved unfeasible to implement. Only recently have sufficiently fast algorithms and computers become available at a reasonable cost that made deconvolution microscopy practical for a more widespread use. The DeltaVision system implemented in this study uses the constrained iteration method developed by Agard et al. (1989). Different algorithms have been developed by other researchers and are used in other systems as well (for a comprehensive listing see Shaw, 1998).

In contrast, confocal microscopes use dual pinhole apertures to restrict unwanted light from reaching the imaging detector (a photo multiplier tube). Out-of-focus light is never collected and, therefore, image resolution is improved. Using pinholes, however, requires using a laser as illumination source since most of the light emitted from the specimen is not imaged and will be lost. This restricts the variety of fluorophors that can be used since lasers produce light with specific wavelengths only. CFP, for example, cannot be excited with standard krypton/argon-ion lasers. Other types of lasers are, however, available that emit light with the required wavelength (for a recent comparative listing of currently commercially available systems, see McAdara, 2000). Resolution is often reduced by a low signal-to-noise ratio due to the discarding of light emitted by the specimen often resulting in "grainy" images as, for example, seen in the image of a gap junction plaque shown in Figure 1B. Other features of confocal microscopes, such as their advantage to examine thick specimens, their photo-bleaching ability, and true section-imaging, as well as additional newly developed technologies such as the Nipko dual-disk scanning technology (UltraView, Perkin Elmer Wallac Inc., Gaitherburg, MD) are clearly of superb value (for reviews see Murray, 1998; McAdara, 2000).

Conventional wide-field fluorescence microscopes collect the entire thickness of the sample in one image, and fluorescence blur will be present. Their main advantages, however, include speed, much lower costs, and simple usage, making them irreplaceable workhorses ideally suited for routine applications (for review see Keller, 1998). Furthermore, an objective lens with an adjustable aperture can be used to restrict the contribution of out-of-focus fluorescence from an image.

Size of Image-Files and Data Handling

Besides the relatively high costs (comparable to an electron microscope) that, in part, are due to the high-precision components required to obtain highly satisfactory results, a substantial drawback of DV micros-

copy today, as we see it, is that it is still a relatively slow technique. This is mainly due to the time-consuming deconvolution and image-processing functions that can take many times longer than the actual imaging process. In part, this is caused by the large data files generated by this technique. For example, a single image of a gap junction plaque, 512 × 512 pixels in size comprises ~ 0.5 Megabytes. Dual-color z-scans consisting of 50 sections, taken with a spacing of 0.2 μm, covering ~ 10 μm, which were generally required to image the entire thickness of a gap junction plaque as the ones shown in Figures 2 and 3, require 50 Megabites of storage. Deconvolved files, volume views, and movie files require similar space when saved uncompressed. This means that three to four of such z-scans including image processing files can easily fill the entire capacity of a CD-ROM, and require several hours to be deconvolved and processed. Time lapse recordings can easily get to a size of 200 Megabites. A dedicated person may fill 50 CDs or more with data in one year! It appears obvious that such amounts of data require a thorough and sophisticated filing and storage system. In our opinion, however, the obtained high-resolution images and many different image-processing capabilities that are offered with the software package are, without doubt, worth the effort.

Spatial Resolution Achieved With DV Microscopy

When HeLa cells were cotransfected with two connexin isotypes that bear different subclass-characteristics, we found that the two connexins assembled into separate domains consisting of either connexin isotype (red and green areas). However, more or less extensive yellow plaque areas were also observed in the unprocessed images as, for example, seen in the gap junction plaques shown in Figure 3 (middle and bottom). The yellow color would suggest a mixing of the two connexin, or channel types in these areas of the plaque. The yellow areas, however, disappeared, or were reduced to narrow borders located only between green and red domains after the images were deconvolved (Fig. 3, middle and bottom). The enhancement of the image resolution by the deconvolution process indicates that domains consisting of mixed channel populations do not exist in these α/β plaques, and the appearance of yellow is an imaging artifact, generated by the limited spatial resolution of classical light microscopy techniques. Ideally, the yellow borderline should disappear completely if different homogenous domains solely adjoin each other. A yellow line will remain, however, if pixels on the photochip of the CCD camera overlap the border region and sense both emission signals.

With the DV microscope system used in this study, we obtained images of gap junction plaques in which a single light sensitive detector field (pixel) on the photochip of the CCD camera corresponded to an area of 44.8 × 44.8 nm when images were collected at maximal magnification (100× lens plus 1.5× auxiliary magnification). This corresponds to an area of approximately 5 × 5 gap junction channels (Revel and Karnowsky, 1967). Over-sampling, in general, increases the resolution possible with the system used (DeltaVision information brochure). However, image resolution will still be limited since resolution is determined by the wavelength of the fluorescent light. In Figure 4A (left panel) gap junction plaques endogenous to glial cells are imaged and compared to a thin section electron micrograph (right panel) of cells imaged at the same final magnification (space bars in both images have the same length and represent 2 μm). Note that the plaques in both images have comparable size. In the deconvolved image shown in Figure 4B (left panels), two gap junction plaques are shown that include nonjunctional membranes (Friend and Gilula, 1972), appearing as dark, circular areas in the fluorescent background of the densely packed gap junction channels. The boxed area is shown below with a higher secondary magnification. Individual pixels are now clearly visible on this image. The upper nonjunctional membrane area marked covers approximately 4 pixels in diameter, corresponding to ~200 nm or ~20 gap junction channels. The two nonjunctional membrane areas are spaced by 2 pixels (~100 nm) only and are clearly separated from each other. A freeze-fracture replica of a gap junction plaque imaged by electron microscopy is shown in comparison (Fig. 4B, right panels). The central circular nonjunctional membrane area measures ~50 nm in diameter, corresponding to ~5 gap junction channels. In a comparable study, Shah et al. (1998) were able to distinguish two proteins, Nup214, and Tpr, which are located ~200 nm apart on the nuclear pore by laser scanning confocal microscopy.

Previously, freeze-fracture electron microscopy was used almost exclusively to study the structural composition of gap junctions. Several of the structural details such as the wavy edges, the nonjunctional membrane areas within the junctional membranes, and smaller aggregates of channels in proximity to a larger aggregate have been seen by this technique as well. However, freeze fracture electron microscopy is only feasible in fixed or cryo preserved cells, provides only a thin section of a fragment of a plaque, and does not allow to characterize the proteins on the image. SDS freeze fracture immuno labeling (Fujimoto et al., 1997) now allows direct labeling of proteins on the replicas but still not in a quantitative manner. Furthermore, several reports have indicated that the fixation process may alter the packing of the gap junction channels. The ultra high resolution that resolves individual gap junction channels, however, is clearly a superb feature of this technique that is of extreme value.

True Colocalization

The colocalization of two different structures or proteins in a cell can be concluded from their overlap on a merged image. This, however, is critically influenced by the resolution of the image and the distance that separates the two structures. If the structures are small, and they are located close to each other, a high image resolution is required to decide if the two structures are truly colocalizing. The term colocalization actually always requires precise definition, since colocalization will always depend on how colocalization is defined. In Figure 5, an example is shown that demonstrates this point. The images show fixed HeLa cells in which the Golgi apparatus was stained with two antibodies directed against the two Golgi marker proteins Mannosidase II (red) and p58K protein (green). DNA in the

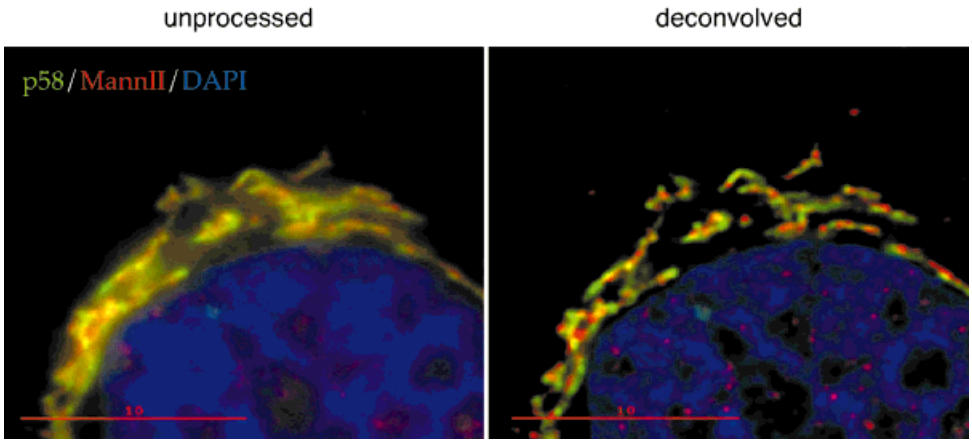

Fig. 5. Colocalization and image resolution. To decide if two structures or proteins truly colocalize is critically dependent on a high image resolution. This is demonstrated in HeLa cells in which the Golgi apparatus was stained with two antibodies recognizing the marker proteins Mannosidase II (red) and p58 K protein (green). Nuclei were stained with DAPI (blue). Cells were imaged with the DV microscope system implemented in this study at maximal magnification (100× lens, plus 1.5× auxiliary magnification) by collecting z-stacks covering the entire thickness of the cells. Images were deconvolved, and volume views rendered. Note that the two marker proteins appear predominantly separated on the deconvolved image (right); however, they appear predominantly colocalizing (yellow) on the unprocessed image (left) due to insufficient spatial resolution. Bars = 10 μm.

nucleus was stained blue with DAPI. Image stacks covering the entire thickness of the cells were collected and volume views were rendered from the unprocessed and the deconvolved image stacks. Note that the two proteins appear predominantly separated (red and green) on the deconvolved volume view, localizing to different Golgi domains. In the unprocessed images, however, they appear as predominantly co-localizing due to the insufficient spatial resolution of the unprocessed images.

Two structures present within an optical section could also be projected on top of each other, and thereby appear as if they were colocalizing. This is demonstrated in the example shown in Figure 6 where regulatory G-proteins and gap junctions were imaged in the presence, and in the absence of oleamide treatment (Clement et al., unpublished data). In Figure 6 (top left), four antibody stained vesicular structures (green, and marked with arrows) appear as if they colocalize with a gap junction plaque (red), since they appear predominantly yellow. When the gap junction plaque is rotated from the view onto its plane into the view onto its edge (Fig. 6, left), it becomes clear that the vesicular structures are spatially separated from the plaque, however, by less than 500 nm. On the other hand, when the vesicular structures are truly attached to the gap junction plaque, a yellow border between green vesicular structures and red gap junction plaques remain in all projections (Fig. 6, right). Image stacks covering the entire thickness of the gap junction plaque were collected at 0.1–μm spacing, images were deconvolved, volume views rendered, and rotated 60° around their longitudinal axis. Images shown in Figures 5 and 6 were acquired at maximal primary magnification (100× lens, plus 1.5× auxiliary magnification), and attached CCD camera was set to binning 1, resulting in the above-mentioned pixel size area of 44.8 × 44.8 nm. This example demonstrates that volume rendering represents a valid method that can be used in addition to optical sectioning to gain better

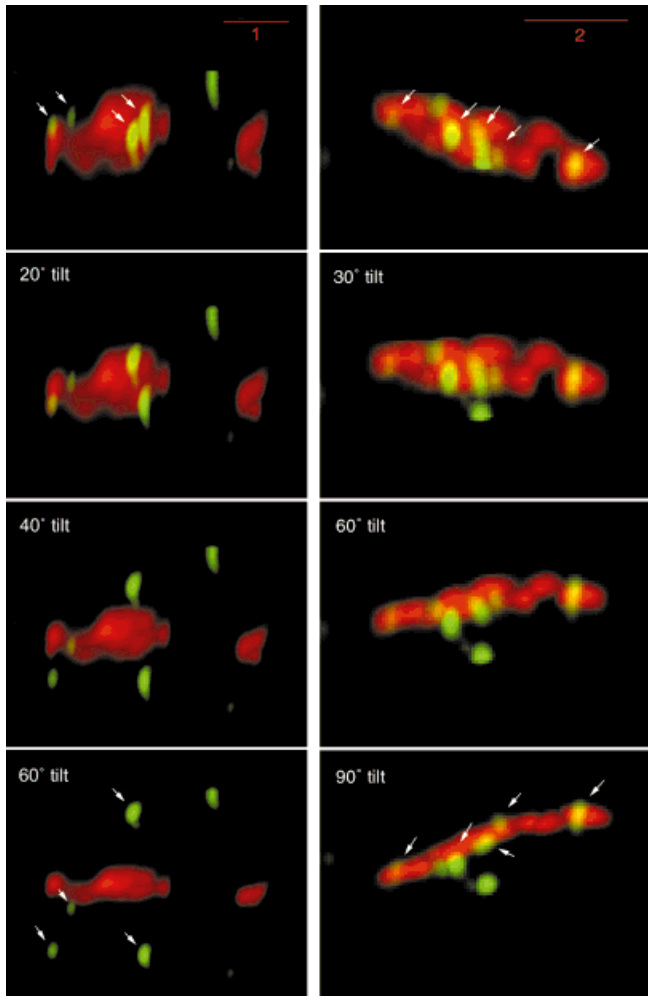

insight into the potential colocalization of two structures.

On the other hand, imaging artifacts could also be misinterpreted so that truly colocalizing structures appear as if they were spatially separated. Light emitted from the specimen passes several different media (specimen, embedding medium, cover glass, immersion oil, glass of the lenses) before it reaches the light detector. Not matching refractive indexes of embedding medium, cover glass, and immersion oil, for example, can cause such artifacts, since light is diffracted differently according to its wavelength when it passes through the media. Specific objectives (Achromats, Fluorites) are corrected for chromatic aberration for blue and red wavelengths, but not for green as Apochromats are (for review see Keller, 1998), and may produce artifacts if such objectives are used for colocalization studies implementing red and green labels (for further reading, see Dunn and Wang, 2000). Finally, poorly aligned scanning mirrors of confocal microscope systems can cause such artifacts as well, since the emitted wavelength signals will be detected in different locations in the PMTs. Awareness of such possible imaging artifacts and appropriate controls should help to ensure proper interpretation of the obtained results.

CONCLUSIONS

In this study, fluorescence DV microscopy and image processing were implemented with live and fixed cells to obtain novel information on the organization, and structural composition of gap junction channel plaques. Gap junctions were visualized in live cells by tagging their structural proteins α_1(Cx43), β_1(Cx32), and β_2(Cx26), with the autofluorescent tracers green fluorescent protein (GFP), and its color variants CFP and YFP. This technology provided true volume reconstructions of gap junction plaques, as they appear in the adjoining membranes between live cells, and resolved details that otherwise could only be seen by ultrastructural analysis of fixed or cryo-preserved cells. Several novel aspects related to the organization and structural composition of gap junctions were revealed that provide novel insight into the function of gap junctions. Specifically, the studies demonstrated that the mode of channel distribution strictly depends on the connexin isotypes. In the future, DV microscopy in combination with fluorescence tagging promises to be very helpful in investigating the biosynthesis, dynamics, and function of gap junctions.

Fig. 6. Rotational volume rendering and image information. Rotated volume views rendered from images of z-section stacks can help to resolve structural interactions and may increase image information. This is demonstrated in two volume views of vesicular structures (stained green and marked with arrows) present in close proximity (**left**), or directly bound (**right**) to gap junction plaques (stained red). In the two top images on the left, the green vesicular structures appear as if they were co-localizing with the red gap junction plaque, since they appear predominantly yellow. When the plaque is rotated around its longitudinal axis it becomes apparent that the vesicular structures are spatially separated, but less than 500 nm from the plaque. When vesicular structures were bound to the plaque, a yellow border remained in all projections (right). "Co-localization" pretended by projecting different structures present in the same optical plain on top of each other can, for example, be resolved using rotational volume rendering. Z-section image stacks spaced 0.1 μm apart were acquired with the deconvolution microscope system implemented in this study at maximal primary magnification (100× lens, plus 1.5× auxiliary magnification), images were deconvolved, volume views rendered and rotated. Individual projections were tilted as shown.

ACKNOWLEDGMENTS

We thank Kelly Moremen, and Norton B. Gilula for providing antibodies and equipment, Angela Clement for providing stained specimens of glial cells, George Klier for providing a freeze-fracture image of a gap junction plaque, Malcolm Wood and The Scripps Research Institute's Core Microscopy Facility for help with thin-section electron microscopy and initial training in deconvolution and confocal microscopy, Peijuan Shen for technical assistance, and Jutta Falk-Marzillier and Lukas Buehler for their scientific discussion and critical suggestions on the manuscript. This work was supported by grant RO1 GM55725 from the National Institute of Health to M.M.F. M.M.F is a former recipient of a Deutsche Forschungsgemeinschaft fellowship Fa 261/1-1.

REFERENCES

Agard DA, Hiraoka Y, Shaw P, Sedat JW. 1989. Fluorescence microscopy in 3 dimensions. Methods Cell Biol 30:353–377.

Andersen JB, Sternberg C, Poulsen LK, Bjorn SP, Givskov M, Molin S. 1998. New unstable variants of green fluorescent protein for studies of transient gene expression in bacteria. Appl Environ Microbiol 64:2240–2246.

Ayoob JC, Turnacioglu KK, Mittal B, Sanger JM, Sanger JW. 2000. Targeting of cardiac muscle titin fragments to the Z-bands and dense bodies of living muscle and non-muscle cells. Cell Motil Cytoskeleton 45:67–82.

Baird GS, Zacharias DA, Tsien RY. Biochemistry, mutagenesis, and oligomerization of DsRed, a red fluorescent protein from coral. Proc Natl Acad Sci USA. 2000 24:97(22):11984–11989.

Brink PR, Cronin K, Banach K, Peterson E, Westphale EM, Seul KH, Ramanan SV, Beyer EC. 1997. Evidence for heteromeric gap junction channels formed from rat connexin43 and human connexin37. Am J Physiol 273:C1386–1396.

Chicurel M. Color-changing protein times gene activity. Science 290: 1478–1479.

Dabiri GA, Turnacioglu KK, Sanger JM, Sanger JW. 1997. Myofibrillogenesis visualized in living embryonic cardiomyocytes. Proc Natl Acad Sci USA 94:9493–9498.

Doyle T, Botstein D. 1996. Movement of yeast cortical actin cytoskeleton visualized in vivo. Proc Natl Acad Sci USA 93:3886–3891.

Dunn KW, Wang E. 2000. Optical aberrations and objective choice in multicolor confocal microscopy. BioTechniques 28:542–550.

Eckert R, Dunina-Barkovskaya A, Hülser DF. 1993. Biophysical characterization of gap junction channels in HeLa cells. Pflügers Arch 205:404–407.

Elfgang C, Eckert R, Lichtenberg-Fraté H, Butterweck A, Traub O, Klein R, Hülser D, Willecke K. 1995. Specific permeability and selective formation of gap junction channels in connexin-transfected HeLa cells. J Cell Biol 129:805–817.

Falk MM. 2000a. Biosynthesis and structural composition of gap junction intercellular membrane channels. Eur J Cell Biol, 79:564–574.

Falk MM. 2000b. Cell-free synthesis for analyzing the membrane integration, oligomerization, and assembly characteristics of gap junction connexins. Methods 20:165–179.

Falk MM, Gilula NB. 1998. Connexin membrane protein biosynthesis is influenced by polypeptide positioning within the translocon and signal peptidase access. J Biol Chem 273:7856–7864.

Falk MM, Kumar NM, Gilula NB. 1994. Membrane insertion of gap junction connexins: polytopic channel forming membrane proteins. J Cell Biol 127:343–355.

Falk MM, Buehler LK, Kumar NM, Gilula NB. 1997. Cell-free synthesis of connexins into functional gap junction membrane channels. EMBO J 10:2703–2716.

Falk MM, Buehler LK, Kumar NM, Gilula NB. 1998. Cell-free expression of functional gap junction channels. In: Werner R, editor. Gap junctions. Amsterdam: IOS Press, p 135–139.

Falk MM. 2000. Connexin-specific distribution within gap junctions revealed in living cells. J Cell Sci 113(Pt 22):4109–4120.

Friend DS, Gilula NB. 1972. Variations in tight and gap junctions in mammalian tissues. J Cell Biol 53:758–776.
Fujimoto K, Nagafuchi A, Tsukita S, Kuraoka A, Ohokuma A, Shibata Y. 1997. Dynamics of connexin, E-cadherin and α-catenin on cell membranes during gap junction formation. J Cell Sci 110:311–322.
Gilula NB, Reeves OR, Steinbach A. 1972. Metabolic coupling, ionic coupling and cell contacts. Nature 235:262–265.
Ginzberg RD, Gilula NB. 1979. Modulation of cell junctions during differentiation of the chicken otocyst sensory epithelium. Dev Biol 68:110–129.
Gross LA, Baird GS, Hoffman RC, Baldridge KK, Tsien RY. 2000. The structure of the chromophore within DsRed, a red fluorescent protein from coral. Proc Natl Acad Sci USA 24:97(22): 11990–11995.
He DS, Jiang JX, Taffet SM, Burt JM. 1999. Formation of heteromeric gap junction channels by connexins 40 and 43 in vascular smooth muscle cells. Proc Natl Acad Sci USA 96:6495–6500.
Heikal AA, Hess ST, Baird GS, Tsein RY, Webb WW. 2000. Molecular spectroscopy and dynamics of intrinisically fluorescent proteins: coral red (dsRed) and yellow. Proc Natl Acad Sci USA 97(22): 11996–12001.
Heim R, Tsien RY. 1996. Engineering green fluorescent protein for improved brightness, longer wavelength and fluorescence resonance energy transfer. Curr Biol 6:178–182.
Heim R, Cubitt AB, Tsien RY. 1995. Improved green fluorescence. Nature 373:663–664.
Holm I, Mikhailov A, Jillson T, Rose B. 1999. Dynamics of gap junctions observed in living cells with connexin43-GFP chimeric protein. Eur J Cell Biol 78:856–866.
Hülser DF, Rehkopf B, Traub O. 1997. Dispersed and aggregated gap junction channels identified by immunogold labeling of freeze-fractured membranes. Exp Cell Res 233:240–251.
Inouye S, Tsuji FI. 1994. *Aequorea* green fluorescent protein: Expression of the gene and fluorescent characteristics of the recombinant protein. FEBS Lett 341:277–280.
Jiang JX, Goodenough DA. 1996. Heteromeric connexons in lens gap junction channels. Proc Natl Acad Sci USA 93:1287–1291.
Jordan K, Solan JL, Dominguez M, Sia M, Hand A, Lampe PD, Laird DW. 1999. Trafficking, assembly, and function of a connexin43-green fluorescent protein chimera in live mammalian cells. Mol Biol Cell 10:2033–2050.
Keller E. 1998. Light microscopy. In: Spector DL, Goldman RD, Leinwand LA, editors. Cells: a laboratory manual, vol 2. Cold Spring Harbor, NY: Cold Spring Harbor Laboratory Press, p. 94.1–94.53.
Kumar NM, Gilula NB. 1996. The gap junction communication channel. Cell 84(3):381–388.
Laird DW, Castillo M, Kasprzak L. 1995. Gap junction turnover, intracellular trafficking, and phosphorylation of connexin43 in brefeldin A-treated rat mammary tumor cells. J Cell Biol 131:1193–1203.
Li X, Zhao X, Fang Y, Jiang X, Duong T, Fan C, Huang CC, Kain SR. 1998. Generation of destabilized green fluorescent protein as a transcription reporter. J Biol Chem 273:34970–34975.
Makowski L, Caspar DLD, Phillips WC, Goodenough DA. 1977. Gap junction structures. J Cell Biol 74:629–645.
Matz VM, Fradkov AF, Labas YA, Savitsky AP, Zaraisky AG, Markelov ML, Lukyanov SA. 1999. Fluorescent proteins from nonbioluminescent Anthozoa species. Nat Biotechnol 17:969–973.
McAdara J. 2000. The resolution solution. Scientist 14:24–26.
McNutt NS, Weinstein RS. 1970. The ultrastructure of the nexus. A correlated thin-section and freeze-cleavage study. J Cell Biol 47: 666–688.
Miesenböck G, deAngelis DA, Rothmann JE. 1998. Visualizing secretion and synaptic transmission with pH-sensitive green fluorescent proteins. Nature 394:192–195.
Milks LC, Kumar NM, Houghten N, Unwin N, Gilula NB. 1988. Topology of the 32-kD liver gap junction protein determined by site-directed antibody localizations. EMBO J 7:2967–2975.
Misteli T, Spector DL. 1997. Applications of the green fluorescent protein in cell biology and biotechnology. Nat Biotech 15:961–964.
Miyawaki A, Llopis J, Heim R, McCaffery J, Adams J, Ikura M, Tsien R. 1997. Fluorescent indicators for Ca^{2+}based on green fluorescent proteins and calmodulin. Nature 388:882–887.
Murray JM. 1998. Confocal microscopy and deconvolution techniques. In: Spector DL, Goldman RD, Leinwand LA, editors. Cells: a laboratory manual Volume 2. Cold Spring Harbor Laboratory Press, p. 96.1–96.23.
Musil LS, Goodenough DA. 1991. Biochemical analysis of connexin43 intracellular transport, phosphorylation, and assembly into gap junction plaques. J Cell Biol 115:1357–1374.
Ormö M, Cubitt AB, Kallio K, Gross LA, Tsien RY, Remington SJ. 1996. Crystal structure of the *Aequorea victoria* green fluorescent protein. Science 273:1392–1395.
Prasher DC, Eckenrode VK, Ward WW, Prendergast FG, Cormier, MJ. 1992. Primary structure of the *Aequorea victoria* green fluorescent protein. Gene 111:229–233.
Rash JE, Staehelin LA, Ellisman MH. 1974. Rectangular arrays of particles on freeze-cleaved plasma membrane are not gap junctions. Exp Cell Res 86:187–190.
Revel JP, Karnowsky MJ. 1967. Hexagonal arrey of subunits in intracellular junctions of the mouse hart and liver. J Cell Biol 33:C7–C12.
Risek B, Klier GF, Gilula NB. 1994. Developmental regulation and structural organization of connexins in epidermal gap junctions. Dev Biol 164:183–196.
Rizutto R, Brini M, Pizzo P, Murgia M, Pozzan T. 1995. Chimeric green fluorescent protein as a tool for visualizing subcellular organelles in living cells. Curr Biol 5:635–642.
Shah S, Tugendreich S, Forbes D. 1998. Major binding sites for the nuclear import receptor are the internal nucleoporin Nup153 and the adjacent nuclear filament protein Tpr. J Cell Biol 141:31–49.
Shaw PJ. 1998. Computational deblurring of fluorescence microscope images. In: Celis JE, editor. Cell biology: a laboratory handbook, vol. 3. San Diego: Academic Press, p 206–217.
Stauffer KA. 1995. The gap junction proteins β_1-connexin (connexin-32) and β_2-connexin (connexin-26) can form heteromeric hemichannels. J Biol Chem 270:6768–6772.
Sullivan R, Lo CW. 1995. Expression of a connexin 43/beta-galactosidase fusion protein inhibits gap junctional communication in NIH3T3 cells. J Cell Biol 130:419–429.
Terskikh A, Fradkov A, Ermakova G, Zaraisky A, Tan P, Kajava AV, Zhao X, Lukyanov S, Matz M, Kim S, Weissman I, Siebert P. 2000. Fluorescent Timer: protein that changes color with time. Science 290(5496):1585–1588.
Tsien RY. 1999. Rosy dawn for fluorescent proteins. Nat Biotechnol 17:956–957.
Unger VM, Kumar NM, Gilula NB, Yeager M. 1999. Three-dimensional structure of a recombinant gap junction membrane channel. Science 283:1176–1180.
Wall MA, Socolich M, Ranganathan R. 2000. The structural basis for red fluorescence in the tetrameric GFP homolog DsRed. Nat Struct Biol 7(12):1133–1138.
Yang TT, Sinai P, Green G, Kitts PA, Chen YT, Lybarger L, Chervenak R, Patterson GH, Piston DW, Kain SR. 1998. Improved fluorescence and dual color detection with enhanced blue and green variants of the green fluorescent protein. J Biol Chem 273:8212–8216.
Yeager M, Unger VM, Falk MM. 1998. Synthesis, assembly and structure of gap junction intercellular channels. Curr Opin Struct Biol 8:517–524.